Generalized Multiscale Inversion for Heterogeneous Problems

Eric T. Chung[1] *, Yalchin Efendiev[2], Bangti Jin[3], Wing Tat Leung[4], and Maria Vasilyeva[5]

[1] *Department of Mathematics, The Chinese University of Hong Kong, Shatin, New Territories, Hong Kong SAR, China.*
[2] *Department of Mathematics & Institute for Scientific Computation (ISC), Texas A&M University, College Station, Texas, USA.*
[3] *Department of Computer Science, University of College London, Gower Street, London WC1E 6BT, UK.*
[4] *Department of Mathematics, Texas A&M University, College Station, TX 77843, USA.*
[5] *Institute for Scientific Computation, Texas A&M University, College Station, TX, USA & Department of Computational Technologies, North-Eastern Federal University, Yakutsk, Republic of Sakha (Yakutia), Russia.*

Abstract. In this work, we propose a generalized multiscale inversion algorithm for heterogeneous problems that aims at solving an inverse problem on a computational coarse grid. Previous inversion techniques for multiscale problems seek a coarse-grid medium properties, e.g., permeability and conductivity, and by doing so, they assume that there exists a homogenized representation of the underlying fine-scale permeability field on a coarse grid. Generally such assumptions do not hold for highly heterogeneous fields, e.g., fracture media or channelized fields, where the width of channels are very small compared to the scale of coarse grids. In these cases, grid refinement can lead to many degrees of freedom, and thus numerically unattractive to apply. The proposed algorithm is based on the Generalized Multiscale Finite Element Method (GMsFEM), which uses local spectral problems to identify non-localized features, i.e., channels (high-conductivity inclusions that connect the boundaries of the coarse-grid block). The inclusion of these features in the coarse space enables one to achieve a good accuracy. The approach is valid under the assumption that the solution can be well represented in a reduced-dimensional space spanned by multiscale basis functions. In practice, these basis functions are non-obervable as we do not identify the fine-scale features of the permeability field. Our inversion algorithm finds the discretization parameters of the resulting system on the coarse grid. By doing so, we identify the appropriate coarse-grid parameters representing the permeability field instead of fine-grid permeability field. We illustrate the potential of the approach by numerical results for fractured media.

AMS subject classifications: 65M32, 65M60

Key words: multiscale inversion, multiscale problem, generalized multiscale finite element method, coarse-grid.

*Corresponding author. *Email addresses:* tschung@math.cuhk.edu.hk (E. Chung), efendiev@math.tamu.edu (Y. Efendiev), bangti.jin@gmail.com (B. Jin), leungwt@math.tamu.edu (W. Leung), vasilyevadotmdotv@gmail.com (M. Vasilyeva)

1 Introduction

In many applications, one has to deal with medium properties of multiple scales and high contrast. For example, in subsurface applications, high-conductivity channels or fractures can appear in multiple locations and have complex geometries. Such features typically have multiple scales, e.g., very small widths and multiple (long) length scales. The related inverse problems include finding permeability (or channel distribution) from noisy and sparse pressure or concentration measurements, and they can be posed either as a regularized least squares formulation and/or within a Bayesian formulation.

There are several challenges when performing inversion using standard approaches (see the monographs [15,26,31,39,40] and references therein for details) for heterogeneous problems. Because of the presence of small scales, one needs to resolve multiple scales properly, which can lead to huge ill-posed systems that are difficult to solve. However, one cannot perform inversion on a coarse grid using standard approaches directly, since the latter implicitly assumes that there is a homogenized model (see, e.g., [16,18,37] for related inverse problems for homogenization). It was shown in [7,11,17] that this assumption is not valid for many practical multiscale problems, even at a low-order approximation. Indeed, because of the presence of high-contrast channels, one cannot use a single permeability or conductivity to represent a coarse-grid block. To remedy these drawbacks, multiple continuum approaches [2,3,32,38,41,42] can be employed instead; however, these approaches require multiple assumptions [8]. Meanwhile, using fine-grid discretizations can lead to many degrees of freedom without a priori knowledge of the locations of these thin features. In this paper, we present a novel generalized multiscale inversion algorithm, which employs our recent multiscale methods and solves inverse problem for discretization parameters rather than for fine-grid permeability fields. Thus by construction, it provides a low-dimensional inverse problem on the coarse grid and avoids many prior assumptions on the fine-grid geometry in order to regularize the inverse problem. The approach is in the spirit of regularization by discretization.

Next, we briefly discuss generalized multiscale methods in the context of inverse problems. We conceptually sketch it in Fig. 1, where we emphasize that one needs appropriate coarse-grid models (with multiple basis functions) for the inversion in order to achieve an accuracy within the error tolerance of the data. For simplicity, we consider a multiscale parabolic equation

$$\frac{\partial u}{\partial t} - \operatorname{div}(\kappa \nabla u) = f, \quad \text{in } \Omega \times (0,T], \tag{1.1}$$

with a homogeneous Dirichlet boundary condition and a suitable initial condition, where $\Omega \subset \mathbb{R}^n$ is an open bounded domain, $T > 0$ is a fixed a final time, and $\kappa_0 \leq \kappa \leq \kappa_1$ is the unknown permeability field that varies over multiple scales with high contrast. Our approach begins with a computational grid, called the coarse grid, which, as usual, does not resolve all the features of the permeability $\kappa(x)$. One standard approach is to seek $\kappa^*(x)$ on a coarse grid directly. However, it automatically assumes that one has a homogenization within a set of admissible permeability fields that we seek. The latter assumption is violated in many important practical applications, including, e.g., identifying fractures (thin high-conductivity features) or channels with extremely low or high conductivities. In these cases, when the thin features are subgrid with respect to the coarse-grid block, homogenization can only provide very inaccurate solutions. Some alternative approaches include multi-continuum, where multiple homogenized coefficients are assigned in each block, which, however, need certain modeling assumptions. In this work, we shall employ

generalized multiscale approaches, where one constructs multiple physically-relevant basis functions in each coarse block from the observational data (in an adaptive manner).

The multiscale method that we employ for the inversion is based on the Generalized Multiscale Finite Element Method (GMsFEM) [7, 11, 12, 17, 23]. We remark that many other multiscale methods have been developed in the literature [4, 9, 13, 19–22, 24, 25, 28, 30, 34–36]. The main idea of the GMsFEM is to construct multiscale basis functions in each coarse block, by solving suitable local spectral problems. The multiscale basis functions are selected based on dominant modes of local spectral problems. The dominant modes can be identified through a spectral gap and the dominant modes correspond to channelized features, i.e., the high-conductivity channels that connect the boundaries of the coarse block. These features cannot be localized and require separate basis functions. If these features are not represented by separate basis functions or represented by fewer basis functions, one can only get very inaccurate numerical solutions. Hence, if one uses only an upscaled permeability (which corresponds to one basis function), the inversion algorithm can only yield an inaccurate estimate.

Our generalized multiscale inversion algorithm formulates the inverse problem for the discretization parameters on a coarse grid directly. The solution to the direct problem is assumed to be represented/captured by several basis functions in each coarse block, where basis functions are not known *a priori*, but to be inferred from the observational data simultaneously. Next, we represent the measurements in terms of coarse-grid parameters, e.g., entries of the stiffness and mass matrices. The latter is feasible under certain assumptions on physical nature of measurements. For example, if the measured quantities can be written on a coarse grid, one can easily represent the observed data via coarse-grid parameters. Note that in our inversion algorithm, we do not identify detailed basis functions, but only some average information that these basis functions will provide. We call these multiscale basis functions *unobservable* and introduce *observable* counterpart, which allows extracting some average information about the solution. Naturally, in the proposed algorithm, one needs certain physical constraints (on the permeabilities etc.) in order to be able to recover useful information, e.g., some elements of stiffness and mass matrices. The proposed inversion method can also be formulated within a Bayesian framework, by imposing a prior on the stiffness and mass matrices generated from a known fine-grid permeability field, and then to sample the resulting posterior probability distribution with Markov chain Monte Carlo (MCMC) in order to quantify the associated uncertainties [14].

In the last part of the paper, we present several numerical examples for flows in fractured media, using a setup for shale gas applications [1], where the true model has fracture distributions that differ from the initial model and the data are coarse-grid pressures. Because of fracture networks, we assume that the model has at most two basis functions in each coarse block and perform inversion. We test the sensitivity of our approach with respect to data noise and measurement location. Moreover, we present adaptive approaches, where multiscale basis functions are used only in selected regions for the purpose of updating.

The rest of the paper is organized as follows. In Section 2, we give some preliminaries about grids, multiscale method, and the setup of the inverse problem. In Section 3, we present our generalized inversion algorithm. Numerical results are presented in Section 4.

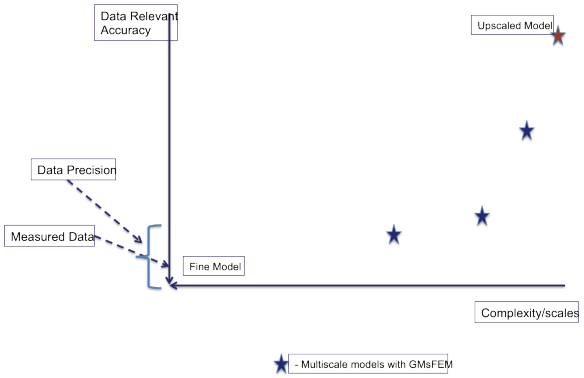

Figure 1: A schematic illustration of the concept of multiscale inversion: The plot shows that one needs appropriate coarse-grid models (with multiple basis functions) for the inversion in order to achieve an accuracy within the data error.

2 Preliminaries

In this section, we describe preliminaries about generalized multiscale finite element methods (GMsFEM), and the setup for the inverse problem.

2.1 Coarse and fine grids

First we introduce the notion of fine- and coarse-grids. Let $\mathcal{T}^H$ be a conforming partition of the domain Ω into finite elements, called coarse grid, with H being the coarse-mesh size. Let N_c be the number of vertices, and N the number of elements in the coarse mesh. Then each coarse element is further partitioned into a connected union of fine-grid blocks, denoted by $\mathcal{T}^h$. The partition $\mathcal{T}^h$ is a refinement of the coarse grid $\mathcal{T}^H$ with the mesh size h. Throughout, it is always assumed that the fine grid is sufficiently fine to resolve the solution. We refer to Fig. 2 for an illustration.

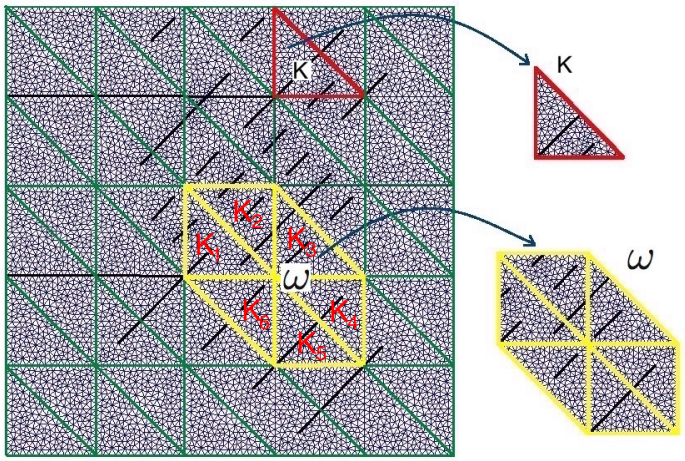

Figure 2: Illustration of the coarse grid $\mathcal{T}^H$, coarse cell K, domain ω (the union of a few coarse cells) and fine grid $\mathcal{T}^h$.

2.2 Multiscale basis functions

The GMsFEM consists of two stages: offline and online. First we describe the online stage. Let $V = H_0^1(\Omega)$. Then the solution u of problem (1.1) satisfies

$$(\frac{\partial u}{\partial t}, v) + a(u,v) = (f,v) \quad \text{for all } v \in V, \tag{2.1}$$

where $a(u,v) = \int_\Omega \kappa \nabla u \cdot \nabla v \mathrm{d}x$, and $(\cdot,\cdot)$ denotes the L^2-inner product on Ω. Let $V_{ms} \subset V$ be the space spanned by all multiscale basis functions, whose construction is to be described in detail below. Then the multiscale solution u_{ms} is defined as: find $u_{ms} \in V_{ms}$ such that

$$a(u_{ms}, v) = (f,v) \quad \text{for all } v \in V_{ms}. \tag{2.2}$$

Next we describe the construction of multiscale basis functions, which is performed on the fine mesh, even though it is not used in our inversion algorithm. In the offline stage, a small dimensional finite element space is constructed to solve the global problem for any input parameter, e.g., right-hand side or boundary condition, on a coarse grid. The snapshot space $V_{H,\text{snap}}^{(i)}$ is first constructed for each generic subregion $\omega_i \subset \Omega$, which involves solving multiple local problems on the fine grid, and each local solution is called a snapshot. The snapshot solutions are then used to compute multiscale basis functions. The ideal snapshot space should provide a fast convergence (i.e., good approximation property in suitable norms) and capture essential problem-relevant constraints on the coarse spaces (e.g., divergence free solutions), while can reduce the cost associated with constructing the offline spaces. One can generate snapshot spaces in several different ways [7], and here we employ harmonic snapshots in an oversampling domain (cf. Fig. 2 for a sketch).

In the harmonic snapshot approach, the snapshot space $V_{H,\text{snap}}^{(i)}$ consists of harmonic extensions of fine-grid functions that are defined on the boundary $\partial\omega_i$. For each fine-grid function $\delta_l^h(x)$, we define $\delta_l^h(x_k) = \delta_{l,k}, \forall x_k \in J_h(\omega_i)$ ($\delta_{l,k}$ is the Kronecker symbol, i.e., $\delta_{l,k} = 1$ if $l = k$ and $\delta_{l,k} = 0$ if $l \neq k$), where the notation $J_h(\omega_i)$ denotes the set of fine-grid boundary nodes on the boundary $\partial\omega_i$ of the subregion ω_i. Then we obtain a snapshot function $\eta_l^{(i)}$ by

$$\mathcal{L}(\eta_l^{(i)}) = 0 \ \text{ in } \omega_i, \quad \eta_l^{(i)} = \delta_l^h(x) \text{ on } \partial\omega_i.$$

The snapshot functions can be computed in an oversampling region ω_i^+ in order to enhance the convergence rate, and further, one can use randomized boundary conditions to further reduce the associated cost [5], in the spirit of randomized singular value decomposition.

The offline space $V_{ms}^{(i)}$ is computed for each subregion ω_i (with elements of the space denoted $\psi_l^{(i)}$) from the snapshot space $V_{H,\text{snap}}^{(i)}$. Specifically, we perform a spectral decomposition in the snapshot space and select the dominant modes (corresponding to the smallest eigenvalues) to construct the offline (multiscale) space $V_{ms}^{(i)}$. The convergence rate of the resulting method is determined by $1/\Lambda_*$, where Λ_* is the smallest eigenvalue that the corresponding eigenvector is not included in the multiscale space $V_{ms}^{(i)}$ [12, 33]. The concrete formulation of the local spectral problem can be motivated from the following error analysis. Note that the global energy error can be decomposed into coarse subdomains. With the energy functional on the subdomain ω denoted by

$a_\omega(u,u)$, i.e., $a_\omega(u,u)=\int_\omega \kappa\nabla u\cdot\nabla u\mathrm{d}x$, we have

$$a_\Omega(u-u_H,u-u_H)\preceq\sum_\omega a_\omega(u^\omega-u_H^\omega,u^\omega-u_H^\omega), \tag{2.3}$$

where ω are coarse regions (ω_i), and u^ω is the localization of the solution. The local spectral problem is chosen to bound the local energy error $a_\omega(u^\omega-u_H^\omega,u^\omega-u_H^\omega)$. Ideally, we look for the subspace V_{ms}^ω such that for any $\eta\in V_{H,\text{snap}}^\omega$, there exists a function $\eta_0\in V_{ms}^\omega$ such that

$$a_\omega(\eta-\eta_0,\eta-\eta_0)\preceq\delta s_\omega(\eta-\eta_0,\eta-\eta_0), \tag{2.4}$$

where $\delta>0$ is a small number and $s_\omega(\cdot,\cdot)$ is an auxiliary bilinear form, which has to be chosen properly to ensure the desired approximation property [12]. The main empirical observation is that with the snapshot spaces chosen suitably, the smallest eigenvalues correspond to the channelized features characteristic of the forward solution [10, 12], and thus it enables our multiscale inversion technique.

2.3 Setup of inverse problem

In the paper, our goal is to find some average information about the fine-scale solution $u_h(x)$ and the permeability field $\kappa(x)$ given measured data, denoted by d. Since our multiscale inversion technique does not identify $\kappa(x)$ and the solution $u_h(x)$ directly, we denote the integrated responses by $\kappa_{ms}(x)$ and $u_{ms}(x)$, where the subscript ms denotes the multiscale inversion. In a Bayesian framework, we can formulate the inverse problem as

$$P(\kappa_{ms}(x),u_{ms}(x)|d)\propto P(d|\kappa_{ms}(x),u_{ms}(x))\pi(\kappa_{ms}(x))\pi(u_{ms}(x)),$$

where $P(d|\kappa_{ms}(x),u_{ms}(x))$ is the likelihood function, $\pi(\kappa_{ms}(x))$ is the prior on multiscale discretization parameters related to the coarse-grid $\mathcal{T}^H$, and $\pi(u_{ms}(x))$ is the prior on the coarse-grid solution. We will describe the likelihood function and these priors more precisely later on. For the data d, we will assume that we measure average pressure over some coarse-grid blocks, for which the special structure allows developing a simple iterative update formula.

3 Multiscale inversion

In this section, we describe the inversion formulation, and the numerical algorithm.

3.1 Inversion formulation

Denote the fine-grid solution by u_h and the coarse-grid solution by

$$u_H=\sum_{i,j}c_{ij}\phi_j^{\omega_i},$$

where $\phi_j^{\omega_i}(x)$ are GMsFEM basis functions defined on the subregion ω_i, and the indices i and j refer to the subregion and the associated basis functions, respectively. These basis functions can approximate the fine-grid solution u_h accurately in the context of the inverse problem. We

shall denote the vector of expansion coefficients c_{ij} by c, and identify the forward solution u_h with the coefficient vector c. Throughout, it is always assumed that the problem has a low-rank reduced dimensional approximation, i.e., very few GMsFEM basis functions can provide a good approximation of the fine-grid solution u_h (in a suitable norm $\|\cdot\|$):

$$\|u_h - u_H\| \approx \text{small}. \tag{3.1}$$

Suppose that we measure the quantity F_{obs} defined by

$$F_{\text{obs}} = G(u_h),$$

where G is a bounded linear mapping. In view of the relation (3.1), we directly have $G(u_h) \approx G(u_H)$. Next, we formulate the inverse problem in terms of the discrete parameters (defined on the coarse grid $\mathcal{T}^H$). Note that the coefficient vector c of the discrete coarse-grid solution u_H takes the following form

$$M\frac{dc}{dt} + Ac = b,$$

with unknown low dimensional matrices A and M (which depend on basis functions $\phi_j^{\omega_i}(x)$ and κ – both are unknown in the inverse context), and the time-dependent vector b is source term. By the linearity of the operator G, we also have

$$F_{\text{obs}} \approx G(u_H) = \sum_{i,j} c_{i,j} G(\phi_j^{\omega_i}).$$

For the proposed multiscale inversion technique, the standing assumption on the measurement operator G is that

$$G(\phi_j^{\omega_i}) = y(c, A, M), \tag{3.2}$$

i.e., the observed response F_{obs} can be expressed in terms of the elements of the stiffness and mass matrices A and M and the coefficient vector c. This assumption holds true for a wide variety of observations, which are averaged quantities over coarse blocks, e.g., pressures or fluxes. In this case, we have

$$F_{\text{obs}} = \mathcal{Y}(c, A, M).$$

We illustrate this general formulation with two more concrete examples. For example, if we observe the average pressure on a coarse block K away from the boundary:

$$y_K = \int_K u_H \mathrm{d}x = c_{ij} \int_K \phi_i^{\omega_j} \mathrm{d}x.$$

To express the given data this in terms of c, A, and M, we recall the entry $(M)_{ij,kl}$ of the mass matrix $(M)_{ij,kl} = \int_\omega \phi_i^{\omega_j} \phi_k^{\omega_l} \mathrm{d}x$. In our numerical studies, we seek the element-wise components of $(M)_{ij,kl}$ for each K (see Fig. 2), denote it by $(M)_{ij,kl}^K$. Then, since the first basis functions form the partition of unity, there holds

$$y_K = c_{ij} \sum_{k=1, l \in \mathcal{I}} (M)_{ij,kl}^K, \qquad G = \mathcal{G}(c, M),$$

where $\mathcal{I}$ is the set of indices for coarse vertices. Similarly, if we observe the average flux (for simplicity, we denote it by y_K) over a coarse block K

$$y_K = \int_K \kappa \nabla u_H \mathrm{d}x = c_{ij} \int_K \kappa \nabla \phi_i^{\omega_j} \mathrm{d}x.$$

Note that $(A)_{ij,kl} = \int_\omega \kappa \nabla \phi_i^{\omega_j} \cdot \nabla \phi_k^{\omega_l} \mathrm{d}x$. Then, one can solve for $\int_K \kappa \nabla u_H \mathrm{d}x$ from $(A)^K_{ij,kl}$, the elements of the stiffness matrix in K corresponding to $k=1$. To do so, we first note that $(A)^K_{ij,1l} = \int_K \kappa \nabla \phi_i^{\omega_j} \cdot \nabla \phi_1^{\omega_l} \mathrm{d}x = \int_K \kappa \nabla \phi_i^{\omega_j} \cdot \nabla \phi^0_{\omega_l} \mathrm{d}x$, where $\phi^0_{\omega_l}$ are linear basis functions. By solving the resulting 2×2 system, we can compute $\int_K \kappa \nabla \phi_i^{\omega_j} \mathrm{d}x$.

Note that in this case, we cannot identify the solution $u(x)$ explicitly, since we do not know the basis functions. However, given the elements (or their estimates) of the stiffness matrix A, we can find some properties of the fine-grid permeability $\kappa(x)$. Upon writing the observation in terms of coarse-grid discretization parameters, the multiscale inverse problem has the following formulation

$$P(c,A,M|d) \propto P(d|c,A,M)\pi(A)\pi(M)\pi(c). \tag{3.3}$$

The priors on A, M, and c can be specified in various ways, depending on the specific application. In our simulations, we use Gaussian priors around a given state generated with a fixed permeability field. In general, one can use a Gaussian mixture field based on several generated permeability fields or priors generated using fine-grid permeability fields as in a Bayesian framework [6]; however, we stress that our objective is to recover coarse-grid parameters. Once we identify c, A, and M, some solution averages can be obtained. To formalize this process, we assume that we can construct a set of observable basis functions $\widetilde{\phi_j^{\omega_i}}$ such that

$$\sum_{i,j} c_{i,j} G(\phi_j^{\omega_i}) \approx \sum_{i,j} c_{i,j} G(\widetilde{\phi_j^{\omega_i}}),$$

or equivalently $G(\phi_j^{\omega_i}) \approx G(\widetilde{\phi_j^{\omega_i}})$. This latter assumption has to be verified case by case for each operator G. Generally, it is necessary for performing inversion on a coarse grid in order to guarantee that the observation can be observed on a coarse-grid solution.

Remark 3.1. When the permeability field $\kappa(x)$ is parameterized or samples of permeability fields are known, we can compute the multiscale basis functions $\phi_i^{\omega_j}$. Then one can compute the fine-grid solution without explicitly finding κ.

Remark 3.2 (One basis function - numerical homogenization)**.** In numerical homogenization, our goal is to find κ^* on a coarse grid. Then the coarse-grid solution u_H satisfies

$$\frac{\partial u_H^*}{\partial t} + \mathcal{L}(\kappa^*, u_H^*) = 0,$$

where $\mathcal{L}$ is an elliptic differential operator depending on κ^*. Assume that we can observe the data F_{obs} based on a coarse-grid solution u_H: $G(u_H^*) = F_{\text{obs}}$. In analogy, we assume that one unobservable basis function can be used to approximate the solution $u_H = \sum_i c_i \phi^{\omega_i}$. Then we can take $\widetilde{\phi^{\omega_i}} = \phi_0^{\omega_i}$, polynomial basis function that has the same linear boundary conditions as multiscale basis functions.

Remark 3.3 (Multi-continuum approach)**.** In the recent work [8], we have discussed the relation between the GMsFEM and multi-continuum approaches. For multi-continuum equations, the generalized multiscale inversion technique reduces to finding parameters in multi-continuum equations. For example, in a simplified case, the coarse-grid equations assume the form

$$\frac{\partial u^*_{i,H}}{\partial t} - div(\kappa^*_i \nabla u^*_{i,H}) + Q_{ij}(u^*_{j,H} - u^*_{i,H}) = 0,$$

where the index i refers to the continua and our goal is to identify κ^*_i and Q_{ij}. The latter can be done using standard inverse problem approaches. As a result, we compute the effective properties of each continua and they cannot be directly related to the fine-grid permeability field. Our approach avoids assumptions of multi-continua approaches and, while as in multi-continua inversion, identifies some average properties about the fine-scale permeability field.

3.2 Numerical algorithm

In practice, the inversion can be performed by solving the following minimization problem

$$J(M,A,u) = \frac{1}{\sigma_M^2}||M - M_0||^2 + \frac{1}{\sigma_A^2}||A - A_0||^2 + \frac{1}{\sigma_F^2}||Fu - g||^2_{L^2(0,T)}, \tag{3.4}$$

where M and A are global mass and stiffness matrices, respectively, and M_0 and A_0 are the corresponding given prior information. This optimization problem can be viewed as computing only the maximum a posteriori estimator of the posterior distribution $P(c,A,M|d)$ defined in (3.3), which represents one computationally attractive way to explore the posterior distribution $P(c,A,M|d)$, by identifying u_h with its coefficient vector c. The benefit of the formulation is that it is deterministic, and can be efficiently minimized. Below, we use Gaussian priors around a state generated with a fixed permeability field (however, in principle, other nonsmooth priors can be employed as well). In general, one can use a Gaussian mixture model based on several generated permeability fields or priors generated by fine-grid permeability fields as in Bayesian models, as mentioned earlier. We remark that the positive scalars σ_M,σ_A and σ_F play the role of regularization parameters, which are constructed to give relative weights of the terms. Choosing proper regularization parameters is a notoriously challenging task in general and depends on the choice of the prior and the specific application, and we refer to [26] for detailed discussions on various ways for selecting a single regularization parameter. Moreover, one needs to select the norms appropriately in (3.4) to guarantee the robustness with respect to the data perturbation [26]. In this work, for simplicity, we employ the discrete quantities and l^2 norms in (3.4), and leave the rigorous studies to future work. In the functional, the operator F is the measurement operator, and g is the observed data. In our numerical simulations, the observed data g is obtained by solving the forward problem on the fine grid, and then apply the operator F to the solution u_h. In particular, for each coarse element K, we have

$$F^K u_h := \bar{u}^K_h(t) \equiv \frac{1}{|K|} \sum_{i=1}^{DOF_K} c^K_i(t) \sum_{j=1}^{DOF_K} m^K_{ij},$$

where the superscript K refers to the coarse element K, $|K|$ denotes the Lebesgue measure of the element K, and DOF_K denotes the number of degree of freedom associated with the element K.

We will solve the optimization problem (3.4) using an iterative procedure. First, we assume that some initial approximations for the local mass and stiffness matrices A_0^K and M_0^K are given. These matrices are found by generating a priori realization and used as a regularization for the low-dimensional inverse problem. Based on these initial conditions, we solve the global forward problem and find an initial approximation $u_0(t)$

$$(A_0, M_0) \to u_0(t),$$

and the corresponding simulated observational data $g_0^K(t)$ is the average pressure in cell K

$$\bar{u}_0^K(t) = \frac{1}{|K|} \sum_{i=1}^{DOF_K} c_{0,i}^K(t) \sum_{j=1}^{DOF_K} m_{ij}^K,$$

The multiscale inversion algorithm proceeds as follows; see Algorithm 1 for the details. The stopping criterion at Step 6 can be taken that the magnitude of the gradient or the change of the value of the objective functional falls below a given tolerance. First, we seek the element-wise components of the stiffness and mass matrices A and M. In this way, we can ensure the symmetry. We iteratively ($n = 1,2,...$) update the local mass matrix M_n^K and local stiffness matrix A_n^K (with the subscript n indicating the iteration index)

$$M_n^K = M_{n-1}^K - \epsilon \delta J_M \quad \text{and} \quad A_n^K = A_{n-1}^K - \epsilon \delta J_A, \tag{3.5}$$

using the previous iterates M_{n-1}^K and A_{n-1}^K, where $\epsilon > 0$ is the step size, and δJ_A and δJ_M denote the derivative of the functional J with respect to A and M, respectively. Further, we generate global mass and stiffness matrices by local matrices and solve the global forward problem

$$(A_n, \quad M_n) \to u_n(t), \tag{3.6}$$

and find average cell pressure

$$\bar{u}_n^K(t) = \frac{1}{|K|} \sum_{i=1}^{DOF_K} c_{n,i}^K(t) \sum_{j=1}^{DOF_K} m_{ij}^K. \tag{3.7}$$

In the gradient descent iteration (3.5), we need the derivatives δJ_M and δJ_A of the functional J with respect to the matrices M and A. To this end, we employ the standard adjoint state technique. In the following, we only give the main steps since the derivation is rather standard [27]. Consider the adjoint problem

$$\frac{\partial w}{\partial t} + \operatorname{div}(\kappa \nabla w) = -F^T(Fu - g), \quad w(T) = 0$$

where F^T is the adjoint of the operator F. Note that the adjoint problem is defined backward in time, and can be solved numerically as usual by a change of variable $t \leftarrow T - t$. Suppose that we represent the adjoint solution w as $\{\lambda_{n-1,i}\}$ in the multiscale basis $\phi_i^{\omega_j}$. Then using the adjoint solution $w(t)$ and the forward solution $u_{n-1}(t)$, the local component $(\delta J_M)_{ij}^K$ of the derivative δJ_M can be computed as

$$(\delta J_M)_{ij}^K = \frac{2}{\sigma_M^2}\left((M_{n-1})_{ij}^K - (M_0)_{ij}^K\right) - \frac{2}{\sigma_F^2}(M_{n-1})_{ij}^K \int_0^T \frac{d\lambda_{n-1,j_g}}{dt} c_{n-1,i_g}, \tag{3.8}$$

where i_g is the corresponding global index. That is, i_g is the global index of the vertex corresponding to the local index i. Similarly, we can compute the derivative δJ_A as

$$(\delta J_A)_{ij}^K = \frac{2}{\sigma_A^2}\left((A_{n-1})_{ij}^K - (A_0)_{ij}^K\right) - \frac{2}{\sigma_F^2}(A_{n-1})_{ij}^K \int_0^T \lambda_{n-1,j_g} c_{n-1,i_g}. \tag{3.9}$$

Algorithm 1 Multiscale inversion algorithm.

1: Give the initial guess (A_0, M_0), the maximum number K of iterations and the step size ϵ;
2: **for** $k = 1,\ldots,K$ **do**
3: Solve for u_k from (A_{k-1}, M_{k-1}) by solving the direct problem;
4: Compute the gradient δJ_A and δJ_M by the adjoint method, cf. (3.8) and (3.9);
5: Update (A_k, M_k) by the gradient descent (3.5);
6: Check the stopping criterion.
7: **end for**

4 Numerical results

Now we illustrate our multiscale inversion technique with flows in fractured media. First, we emphasize that the proposed method is general and can be used for general heterogeneous high-contrast problems. It is especially suitable for channelized and fractured media. In channelized media problems, the locations of high-conductivity channels are unknown and the channels can have very small thickness, which calls for very small fine grid everywhere if the inversion is directly performed on the fine grid and thus it can be very expensive. Meanwhile, channelized media problems can be represented on the coarse grid using GMsFEM and multiple basis functions. Using multiple basis functions within GMsFEM (un-observable basis functions), we can perform inversion efficiently. For these problems, homogenization-based approaches (identifying grid-block conductivities) does not work, as discussed earlier. Fractured media can be considered as channelized media in the limit when channel thickness goes to zero, while the conductivity is very high. In this case, the channels are written as low dimensional high-conductivity regions. These models are written in a discrete formulation since the fractures have zero widths.

In our numerical experiment, we take the computational domain $\Omega = [0,1]^2$. Fractures have high conductivities, very small width, and are modeled as high-conductivity lines; see [8] for details. To describe the model problem, we divide the domain Ω into the fracture and the matrix region $\Omega = \Omega_m \oplus_i d_i \Omega_{f,i}$, where the subscripts m and f denote the matrix and fracture regions, respectively. The fracture regions $\Omega_{f,i}$ consist of lines in 2D (and low-dimensional objects in higher dimensions). We denote by d_i the aperture of the i-th fracture, where i is the index of the fractures. The aperture of the fracture determines its conductivity and we denote by $\kappa_{f,i}$ the conductivity (permeability) of the i-th fracture. The matrix domain Ω_m is a two-dimensional domain.

The bilinear form for flow in fractured media is given by

$$\int_{\Omega_m} \frac{\partial u_h}{\partial t} v_h dx + \int_{\Omega_m} \kappa_m \nabla u_h \cdot \nabla v_h dx + \sum_i \int_{\Omega_{f,i}} \kappa_{f,i} \nabla_f u_h \cdot \nabla_f v_h dx = \int_\Omega f v_h dx, \tag{4.1}$$

where v_h is the fine-grid finite element function, ∇_f is the derivative along the fracture lines, and κ_m and $\kappa_{f,i}$ are the matrix and fracture permeabilities ($i = 1,...,N$), respectively. The fracture

permeability include the aperture information d_i. Problem (4.1) can be written into the variational form (2.1).

We consider the coarse mesh that contains 121 vertices and 200 cells. We use the following parameters

- $k_m = 10^{-3}$ and $k_f = 10^2$,
- $u = 0$ on the left boundary ($x_1 = 0$), no flow on the remaining boundaries ($\kappa \nabla u \cdot n = 0$), and $u(t = 0, x) = 1$,
- $f = 0$ and $t_{max} = 10$ with 10 time steps.

To set the prior information, the initialization, and for the comparison with the fine-grid solutions, we use the fine mesh, which contains 6297 vertices and 12352 cells for Case 1. For Case 2, we have 7908 vertices and 15574 cells. For Case 3, fine mesh with 7891 vertices and 15540 cells. The fine meshes for all three cases are depicted in Fig. 3. In Fig. 4, we show the adaptive regions, where we perform updates to the matrices, and unless otherwise stated, these regions are used in all the numerical experiments with the proposed inversion technique below. Further, unless otherwise stated, the step length ϵ in the iteration (3.5) is fixed at $\epsilon = 10^{-12}$.

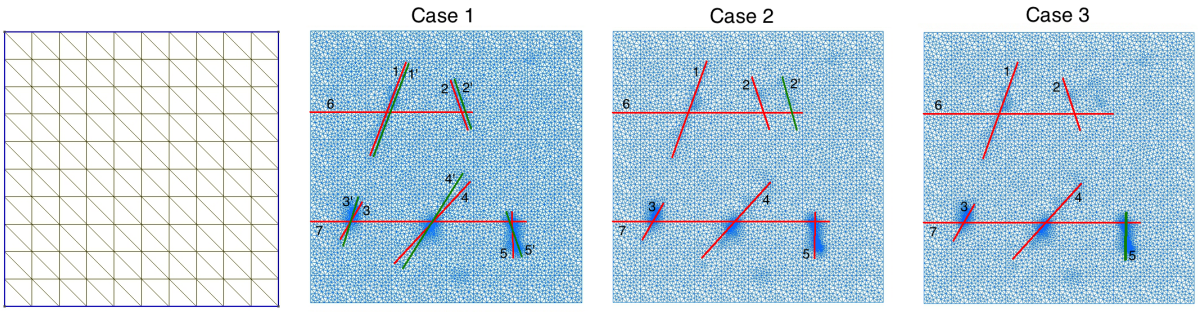

Figure 3: Coarse and fine grids for Cases 1-3. In the figure, red color indicates exact fractures, and the green color is for moved fractures. Case 1 has 3 rotated and 2 shifted fractures, Case 2 has 1 shifted fracture with large distance (second) and Case 3 has 1 removed fracture (fifth).

To evaluate the proposed approach, we first present the following numerical results: the average fine-grid solution, the initial condition and the final solution. All the results are obtained with the following parameter setting: $\sigma_M = \sigma_A = 1.0$ and $\sigma_F = 10^4$, which are determined in a trial and error manner. In Figs. 5, 12 and 14 for the three cases, we present the numerical solutions. It is observed that the recovered solutions are always fairly close to the exact one, indicating the accuracy of the proposed approach.

In Figs. 6, 7, 13 and 15, we present the L^2 errors with respect to the space variable as a function of time t and the residual (functional value) J given in (3.4). In Fig. 6, the cell average solution refers to the fine grid solution averaged on the coarse element K. The L^2 error decreases with the time t, and in the absence of data noise, it also decreases as the iteration proceeds. Further, with more multiscale basis functions in the inversion, the L^2 error is also smaller. We always observe that the residual decreases as the number of iterations grows. The monotone decrease of the residual indicates that the iteration (3.5) is indeed minimizing the functional J.

Next we illustrate the sensitivity of the numerical results by the multiscale inversion algorithm with respect to various algorithmic parameters. In Fig. 8 we present the result for two different

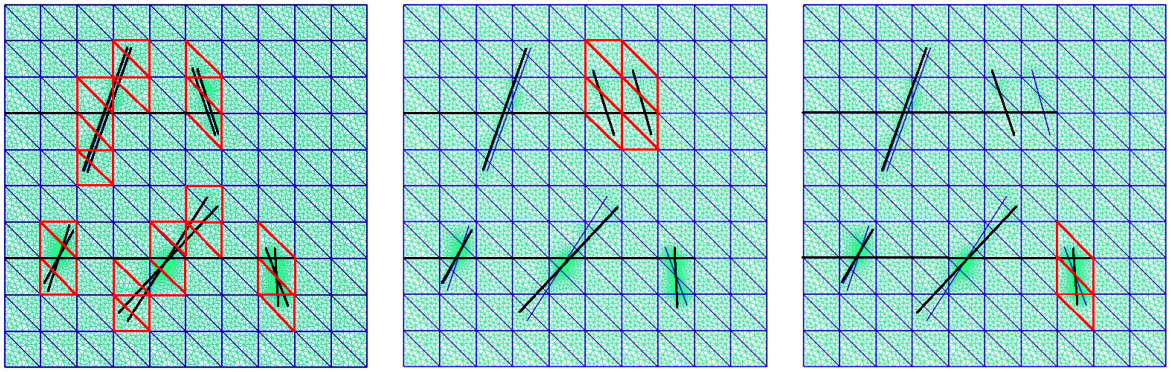

(a) case 1 (b) case 2 (c) case 3

Figure 4: The regions for (adaptive) inversion update for the three cases: The coarse cells in red indicate the corresponding entries of the matrices to be updated.

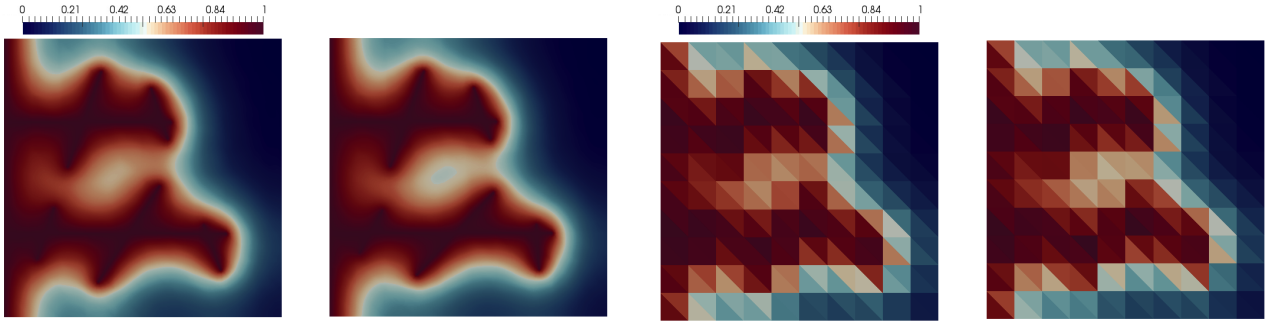

(a) multiscale solution on fine grid (b) 4 multiscale basis functions, adaptive inverse

Figure 5: Numerical results Case 1: (a) multiscale solution for u_0 (left) and exact (right), and (b) cell average solution for initial condition M_0, A_0 (left) and solution after 100 iterations (right).

step lengths $\epsilon = 10^{-12}$ and $\epsilon = 10^{-13}$, where the mass and stiffness matrices are updated adaptively in selected regions and also over the whole computational domain. One observes that the errors and residuals are comparable when the iteration reaches convergence, but with a larger step size can greatly speedup the convergence of the algorithm (whenever it does not violate the step size restriction, as usual for gradient descent type algorithms). Further, the results for the adaptive local update and all cells update of the mass matrices are comparable with each other. Thus the inversion with only local update in the selected regions affects little the reconstruction results. However, numerically, we observe that the local update is much more stable than the global update, e.g., a larger step size ϵ, due to the fact that the local update involves much few unknowns. In Fig. 9, we present the numerical results for the case of observational data contaminated with different amount of noise. It is observed that the results are fairly stable with respect to the present of data noise, up to 100 iterations, due to the priors we specified on the discrete parameters, clearly indicating the stability of the regularized formulation. Naturally, the error and residual increases with the noise level. Last, our inversion algorithm essentially employs local data to update the local coarse grid directly, and thus it is expected that the algorithm can work well as long as the related local data over the interested region is available. This is confirmed by the numerical results

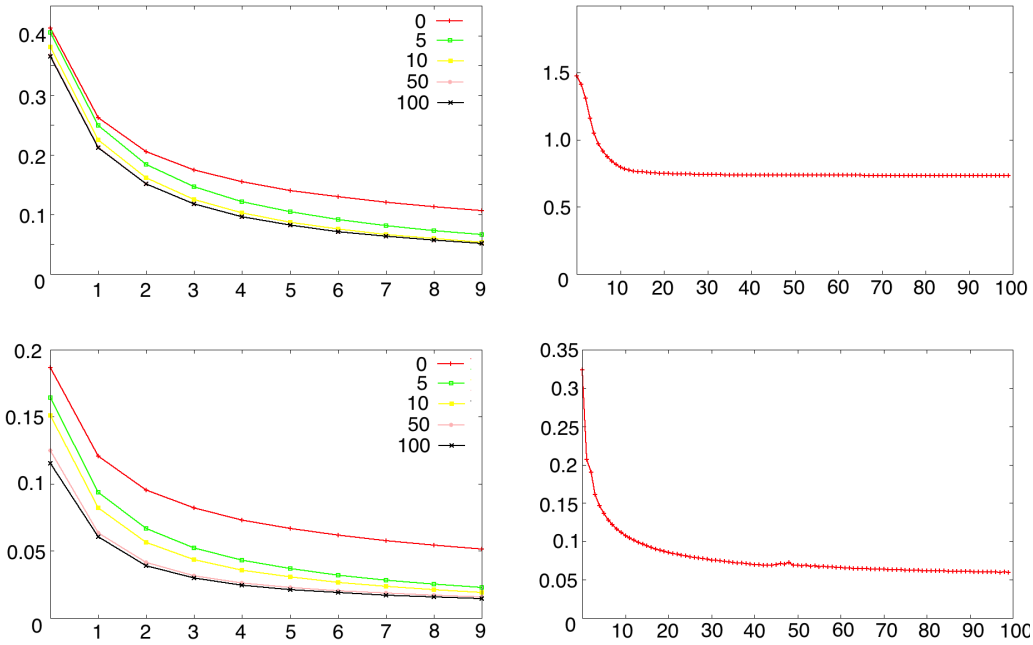

(a) L^2 error v.s. time (b) J v.s. iteration

Figure 6: Numerical results for Case 1 with 2 (top) or 4 (bottom) multiscale basis functions: (a) the L^2 error for cell average v.s. time t at different iterations, and (b) the functional value J v.s. iteration index.

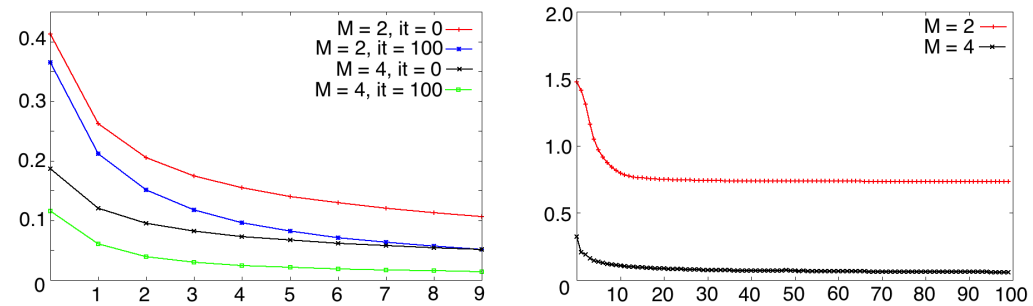

(a) L^2 error v.s. time (b) J v.s. iteration

Figure 7: Numerical results for Case 1, using 2 or 4 multiscale basis functions: (a) L^2 error for cell average v.s. time t, and (b) the functional value J v.s. the iteration index.

in Figs. 10 and 11. However, with sparser data available, a stronger regularization is needed to maintain the stability of the algorithm, and more informative priors, e.g., sparsity or total variation, may be imposed [26, 29, 39].

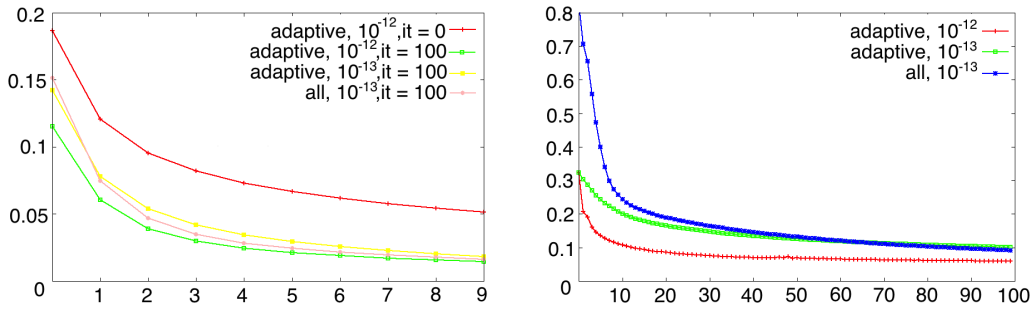

(a) L^2 error v.s. time (b) J v.s. iteration

Figure 8: Numerical results for Case 1, using 4 multiscale basis functions: (a) L^2 error for cell average v.s. time t, and (b) the functional value J v.s. iteration index. Different iteration parameter $\epsilon = 10^{-12}$ and 10^{-13}. Adaptive and all cells local mass matrices updating.

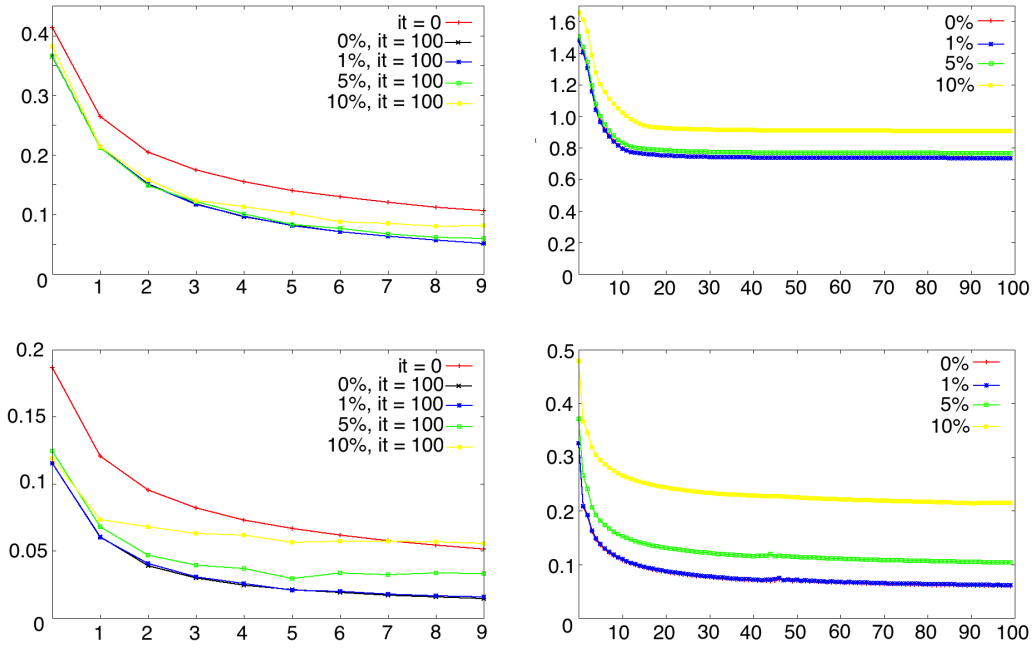

(a) L^2 error v.s. time (b) J v.s. iteration

Figure 9: Numerical results for Case 1 with noisy data g, $g^K(t) = (1+\delta r)g^K(t)$ ($r \in [-1,1]$ is random number and $\delta = 1\%$, 3% , 5% or 10%) with 2 (top) or 4 (bottom) multiscale basis functions: (a) the L^2 error for cell average v.s. time, and (b) the functional value J v.s. iteration index.

5 Conclusions

In this work, we have developed a generalized multiscale inversion algorithm for heterogeneous problems. It is based on the generalized multiscale finite element method (GMsFEM), where one constructs multiscale basis functions to capture the non-localizable features, and the algorithm assumes that the problem admits a reduced-order model on a coarse grid. Then, instead of seek-

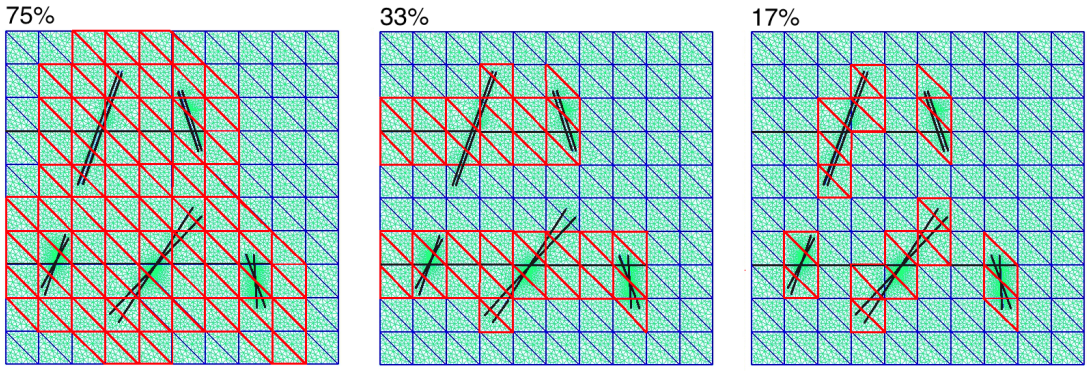

Figure 10: The observation data g^K for Case 1, given in some cells indicated in red.

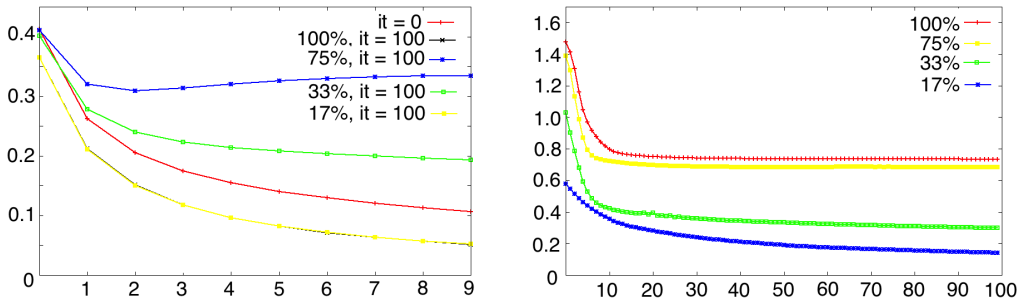

(a) L^2 error v.s. time (b) J v.s. iteration index

Figure 11: Numerical results for Case 1 using 4 multiscale basis functions, with different amount of observational data g^K in some cells shown in Fig. 10: (a) the L^2 error for cell average v.s. time t, and (b) the functional value J v.s. the iteration index.

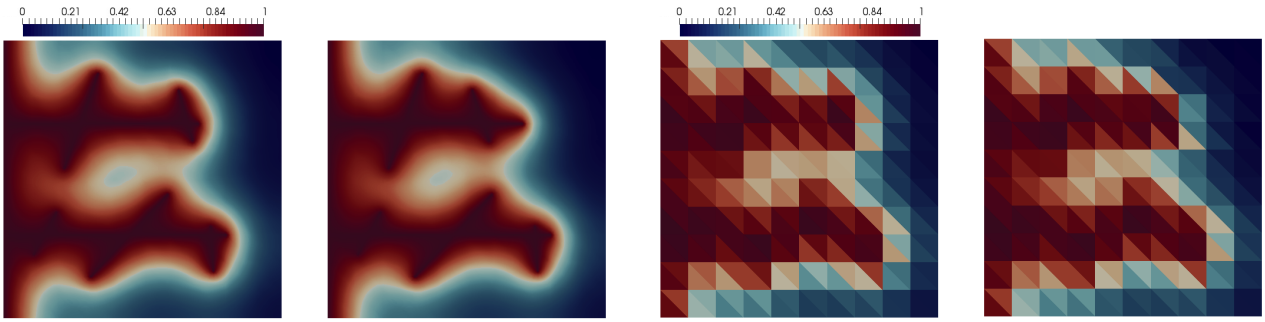

(a) multiscale solution on fine grid (b) 4 multiscale basis functions, adaptive inverse

Figure 12: Numerical results for Case 2: (a) multiscale solution for u_0 (left) and exact (right), and (b) cell average solution for initial condition M_0, A_0 (left) and solution after 100 iterations (right).

ing coarse-grid permeabilities, we seek the discretization parameters that are obtained from the GMsFEM formulation. Our approaches are especially suitable for problems with fractures or high-conductivity channels, when upscaling the permeability can result in very large errors. Thus, it is important to consider a more general multiscale approach. In our approach, we do not compute

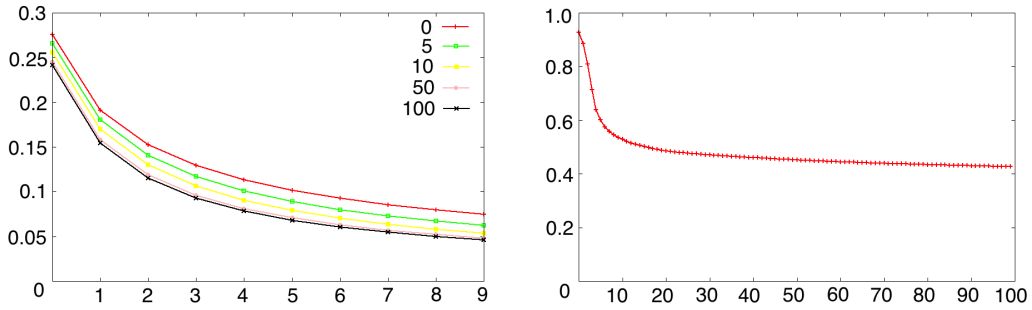

(a) L^2 error v.s. time (b) J v.s. iteration

Figure 13: Numerical results for Case 2, using 4 multiscale basis functions: (a) L^2 error for cell average v.s. time t at different iterations, and (b) the functional value J v.s. the iteration index.

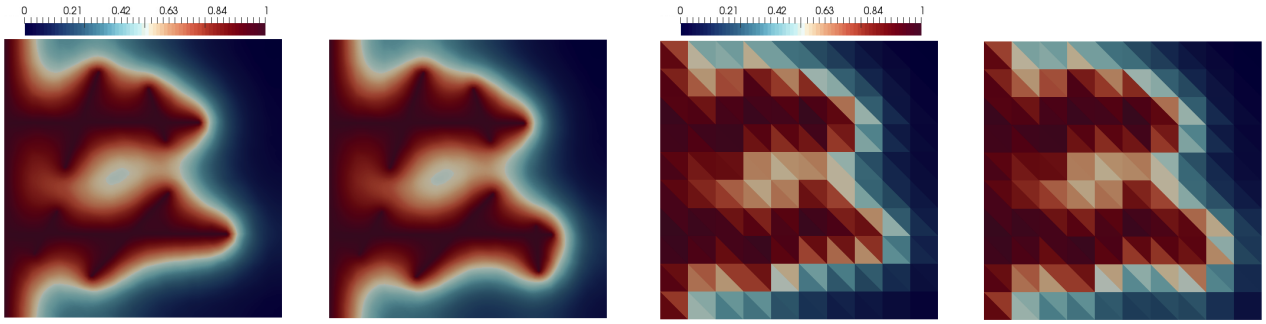

(a) multiscale solution on fine grid (b) 4 multiscale basis functions, adaptive inverse

Figure 14: Numerical results for Case 3: (a) multiscale solution for u_0 (left) and exact (right), and (b) cell average solution for initial condition M_0, A_0 (left) and solution after 100 iterations (right).

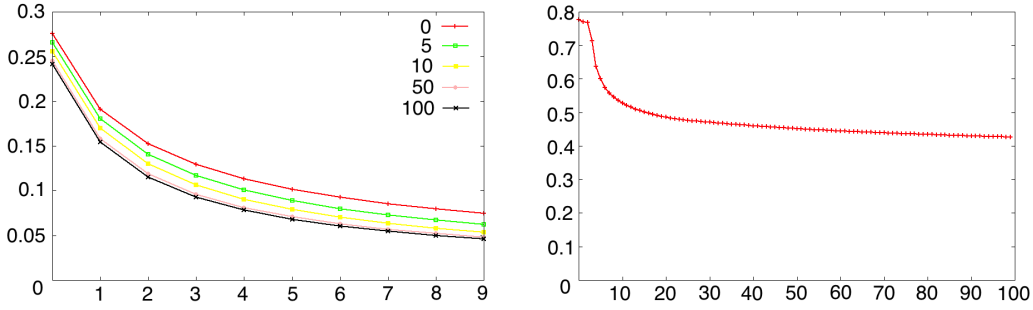

(a) L^2 error v.s. time (b) J v.s. iteration

Figure 15: Numerical results for Case 3 using 4 multiscale basis functions: (a) L^2 error for cell average v.s. time t at different iterations, and (b) the functional value J v.s. the iteration index.

multiscale basis functions and do not recover the fine-scale permeability field. Instead, we compute the averaged coarse-grid discretization parameters, i.e., integrated responses corresponding to unknown multiscale basis functions. We have discussed various regularizations and a Bayesian framework, as well as the important ingredients of the inversion algorithm, and illustrated the ap-

proach with numerical results for fractured media. Our numerical experiments clearly illustrate the feasibility and significant potential of the approach for inverse problems for heterogeneous problems, and it motivates a rigorous mathematical analysis of the proposed approach.

Acknowledgements

MV's work is supported by the grant of the Russian Scientific Found (17-71-20055). YE would like to thank the partial support from NSF 1620318, the U.S. Department of Energy Office of Science, Office of Advanced Scientific Computing Research, Applied Mathematics program under Award Number DE-FG02-13ER26165 and National Priorities Research Program grant NPRP grant 7-1482-1278 from the Qatar National Research Fund. YE would also like to acknowledge the support of Mega-grant of the Russian Federation Government (N 14.Y26.31.0013). EC's research is partially supported by the Hong Kong RGC General Research Fund (Project: 14301314) and the CUHK Direct Grant for Research 2015-16.

References

[1] I. Y. Akkutlu, Y. Efendiev, and M. Vasilyeva. Multiscale model reduction for shale gas transport in fractured media. *Comput. Geosci.*, 20(5):953–973, 2016.

[2] T. Arbogast, J. Douglas, Jr., and U. Hornung. Derivation of the double porosity model of single phase flow via homogenization theory. *SIAM J. Math. Anal.*, 21(4):823–836, 1990.

[3] G. I. Barenblatt, I. P. Zheltov, and I. N. Kochina. Basic concepts in the theory of seepage of homogeneous liquids in fissured rocks [strata]. *J. Appl. Math. Mech.*, 24(5):1286–1303, 1960.

[4] F. Brezzi, L. P. Franca, T. J. R. Hughes, and A. Russo. $b = \int g$. *Comput. Methods in Appl. Mech. and Engrg.*, 145:329–339, 1997.

[5] V. M. Calo, Y. Efendiev, J. Galvis, and G. Li. Randomized oversampling for generalized multiscale finite element methods. *Multiscale Model. Simul.*, 14(1):482–501, 2016.

[6] P. Chen, N. Zabaras, and I. Bilionis. Uncertainty propagation using infinite mixture of Gaussian processes and variational Bayesian inference. *J. Comput. Phys.*, 284:291–333, 2015.

[7] E. Chung, Y. Efendiev, and T. Y. Hou. Adaptive multiscale model reduction with generalized multiscale finite element methods. *J. Comput. Phys.*, 320:69–95, 2016.

[8] E. T. Chung, Y. Efendiev, T. Leung, and M. Vasilyeva. Coupling of multiscale and multi-continuum approaches. *GEM Int. J. Geomath.*, 8(1):9–41, 2017.

[9] D. Cortinovis and P. Jenny. Iterative galerkin-enriched multiscale finite-volume method. *Journal of Computational Physics*, 277:248–267, 2014.

[10] Y. Efendiev and J. Galvis. A domain decomposition preconditioner for multiscale high-contrast problems. In *Domain Decomposition Methods in Science and Engineering XIX*, volume 78 of *Lect. Notes Comput. Sci. Eng.*, pages 189–196. Springer, Heidelberg, 2011.

[11] Y. Efendiev, J. Galvis, and T. Y. Hou. Generalized multiscale finite element methods (GMsFEM). *J. Comput. Phys.*, 251:116–135, 2013.

[12] Y. Efendiev, J. Galvis, and X.-H. Wu. Multiscale finite element methods for high-contrast problems using local spectral basis functions. *J. Comput. Phys.*, 230(4):937–955, 2011.

[13] Y. Efendiev and T. Hou. *Multiscale Finite Element Methods: Theory and Applications*. Springer, 2009.

[14] Y. Efendiev, B. Jin, M. Presho, and X. Tan. Multilevel Markov chain Monte Carlo method for high-contrast single-phase flow problems. *Commun. Comput. Phys.*, 17(1):259–286, 2015.

[15] H. W. Engl, M. Hanke, and A. Neubauer. *Regularization of Inverse Problems*. Kluwer, Dordrecht, 1996.

[16] C. Frederick and B. Engquist. Numerical methods for multiscale inverse problems. *Commun. Math. Sci.*, 15(2):305–328, 2017.

[17] J. Galvis and Y. Efendiev. Domain decomposition preconditioners for multiscale flows in high contrast media: reduced dimension coarse spaces. *Multiscale Model. Simul.*, 8(5):1621–1644, 2010.
[18] M. Gulliksson, A. Holmbom, J. Persson, and Y. Zhang. A separating oscillation method of recovering the *G*-limit in standard and non-standard homogenization problems. *Inverse Problems*, 32(2):025005, 23, 2016.
[19] H. Hajibeygi, D. Karvounis, and P. Jenny. A loosely coupled hierarchical fracture model for the iterative multiscale finite volume method. *Society of Petroleum Engineers. doi:10.2118/141991-MS*.
[20] H. Hajibeygi, D. Karvounis, P. Jenny, et al. A loosely coupled hierarchical fracture model for the iterative multiscale finite volume method. In *SPE Reservoir Simulation Symposium*. Society of Petroleum Engineers, 2011.
[21] H. Hajibeygi, D. Kavounis, and P. Jenny. A hierarchical fracture model for the iterative multiscale finite volume method. *Journal of Computational Physics*, 230(4):8729–8743, 2011.
[22] T. Hou and X. Wu. A multiscale finite element method for elliptic problems in composite materials and porous media. *J. Comput. Phys.*, 134:169–189, 1997.
[23] T. Y. Hou and X.-H. Wu. A multiscale finite element method for elliptic problems in composite materials and porous media. *J. Comput. Phys.*, 134(1):169–189, 1997.
[24] T. Hughes. Multiscale phenomena: Green's functions, the dirichlet-to-neumann formulation, subgrid scale models, bubbles and the origins of stabilized methods. *Comput. Methods Appl. Mech Engrg.*, 127:387–401, 1995.
[25] T. Hughes, G. Feijóo, L. Mazzei, and J.-B. Quincy. The variational multiscale method - a paradigm for computational mechanics. *Comput. Methods Appl. Mech Engrg.*, 127:3–24, 1998.
[26] K. Ito and B. Jin. *Inverse Problems: Tikhonov Theory and Algorithms*. World Scientific Publishing Co. Pte. Ltd., Hackensack, NJ, 2015.
[27] K. Ito and K. Kunisch. *Lagrange Multiplier Approach to Variational Problems and Applications*. SIAM, Philadelphia, PA, 2008.
[28] P. Jenny, S. Lee, and H. Tchelepi. Multi-scale finite volume method for elliptic problems in subsurface flow simulation. *J. Comput. Phys.*, 187:47–67, 2003.
[29] B. Jin and P. Maass. Sparsity regularization for parameter identification problems. *Inverse Problems*, 28(12):123001, 70, 2012.
[30] R. Juanes and T. W. Patzek. A variational multiscale finite element method for multiphase flow in porous media. *Finite Elements in Analysis and Design*, 41(7-8):763–777, 2005.
[31] J. Kaipio and E. Somersalo. *Statistical and Computational Inverse Problems*. Springer-Verlag, New York, 2005.
[32] H. Kazemi, L. S. Merrill Jr, K. L. Porterfield, and P. R. Zeman. Numerical simulation of water-oil flow in naturally fractured reservoirs. *SPE Journal*, 16(6):317–326, 1976.
[33] G. Li. Low-rank approximation to heterogeneous elliptic problems. *Multiscale Model. Simul.*, page in press, 2017.
[34] I. Lunati and P. Jenny. Multi-scale finite-volume method for highly heterogeneous porous media with shale layers. In *Proceedings of the 9th European Conference on the Mathematics of Oil Recovery (ECMOR)*, Cannes, France, 2004.
[35] A. Målqvist and D. Peterseim. Localization of elliptic multiscale problems. *Mathematics of Computation*, 83(290):2583–2603, 2014.
[36] J. Nolen, G. Papanicolaou, and O. Pironneau. A framework for adaptive multiscale method for elliptic problems. *SIAM J. Multiscale Modeling and Simulation*, 7:171–196, 2008.
[37] J. Nolen, G. A. Pavliotis, and A. M. Stuart. Multiscale modeling and inverse problems. In *Numerical Analysis of Multiscale Problems*, volume 83 of *Lect. Notes Comput. Sci. Eng.*, pages 1–34. Springer, Heidelberg, 2012.
[38] K. Pruess and T. N. Narasimhan. On fluid reserves and the production of superheated steam from fractured, vapor-dominated geothermal reservoirs. *J. Geophys. Res. Solid Earth*, 87(B11):9329–9339, 1982.
[39] T. Schuster, B. Kaltenbacher, B. Hofmann, and K. S. Kazimierski. *Regularization Methods in Banach*

Spaces. Walter de Gruyter GmbH & Co. KG, Berlin, 2012.

[40] A. Tarantola. *Inverse Problem Theory and Methods for Model Parameter Estimation*. SIAM, Philadelphia, PA, 2005.

[41] J. E. Warren and P. J. Root. The behavior of naturally fractured reservoirs. *SPE Journal*, 3(3):245–255, 1963.

[42] Y.-S. Wu and K. Pruess. A multiple-porosity method for simulation of naturally fractured petroleum reservoirs. *SPE Res. Eng.*, 3(1):327–336, 1988.